The Role of Extracellular Vesicles Secreted From Thermal Stress-Induced Adipose-Derived Stem Cells on Bone Regeneration

Zeynep Akdeniz-Dogan, MD,[*] Samet Sendur, MD,[†] Betul Karademir-Yilmaz, PhD,[‡] Onur Bugdayci, MD,[#] Ozlem Tugce Cilingir-Kaya, PhD,[¶] Ayse M. Yilmaz-Goler, PhD,[‡] Oguzhan Gunduz, PhD,[**] and Ozhan B. Celebiler, MD[*]

Purpose: Extracellular vesicles (EVs) are responsible for intercellular communication. Mesenchymal stem cell-derived vesicles have been shown to have similar properties as functional mesenchymal stem cells. The aim of this study was to compare the therapeutic benefit of EVs obtained from adipose tissue-derived stem cells (ADSC) on bone repair whereas using ß-tricalcium phosphate (ß-TCP) biomaterial as a carrier.

Materials and Method: A single critical size bone defect of 8 mm in diameter was created on the right side of rat calvarium using a custom-made punch needle. Animals were randomly divided into 5 groups: group 1 (no treatment), group 2 (bone graft), group 3 (ß-TCP + ADSC), group 4 (ß-TCP + EV), group 5 (ß-TCP). Eight weeks later, animals were sacrificed and histologic and radiologic evaluation was performed.

Results: Semiquantitative histologic scoring demonstrated significantly higher bone regeneration scores for groups 2, 3, and 4 compared to group 1. Radiologic imaging showed significantly higher bone mineral density for groups 2, 3, and 5 compared to group 1. There were no significant differences between treatment groups in either histologic or radiologic scoring.

Conclusions: Our data showed that EVs provided from thermally induced ADSCs did not show any significant difference in bone regeneration when compared to ADSCs themselves. Future studies should focus on determining the optimum amount and content of EV application since these vary significantly depending on the microenvironment.

From the *Department of Plastic Reconstructive and Aesthetic Surgery, Marmara University School of Medicine; †Department of Plastic Reconstructive and Aesthetic Surgery, Umraniye Training and Research Hospital; ‡Department of Biochemistry, Marmara University School of Medicine/Genetic and Metabolic Diseases Research and Investigation Center, Marmara University; #Department of Radiology; ¶Department of Histology and Embryology, Marmara University School of Medicine; and **Department of Metalurgical and Materials Engineering, Faculty of Technology, Marmara University, Istanbul, Turkey.

Received November 13, 2020.
Accepted for publication June 7, 2021.

Address correspondence and reprint requests to Zeynep Akdeniz-Dogan, MD, Marmara University School of Medicine, Başibüyük Campus, Başibüyük Mah. Maltepe Başibüyük Yolu Sok. No: 9/2, Maltepe, Istanbul 34854, Turkey; E-mail: zeynepakdeniz@gmail.com

This project has been supported by the Marmara University Scientific Research Fund grant number SAG-B-110117-0002.
The authors report no conflicts of interest.

Copyright © 2021 by Mutaz B. Habal, MD

ISSN: 1049-2275
DOI: 10.1097/SCS.0000000000007901

Key Words: Adipose-derived stem cell, bone regeneration, extracellular vesicle

(*J Craniofac Surg* 2021;32: 2245–2251)

Bony reconstruction of the maxillofacial defects following trauma or tumor surgery are best managed with autologous bone grafts or flaps. This may be challenged by donor site availability or late resorption of bone grafts. More recently multiple biomaterials have been introduced for repair and regeneration of bony defects. ß-Tricalcium phosphate (ß-TCP), which is highly compatible and completely degradable in vivo[1] is already in clinical use for bone repair.[2,3] However it has been shown to lack osteoinductive activity.[4,5]

Mesenchymal stem cells (MSCs) are multi-potent cells with the capacity of differentiating into different cells.[6–13] Although MSCs have been a topic of great interest in the field of regenerative medicine, there is still concern regarding safety and regulations for actual clinical use. Mesenchymal stem cells have been demonstrated to have positive effects on tissue repair by stimulating the activity of the surrounding cells.[14,15] Adipose tissue-derived stem cells (ADSCs), which are capable of differentiating into osteoblasts, chondrocytes, endothelium, and monocytes,[16] can be found in abundance and easily harvested from the fatty tissue. Moreover, ß-TCP has the capacity to stimulate differentiation of ADSCs into osteoblastic phenotype.[17] Mesenchymal stem cells 'role in tissue repair and regeneration is thought to depend more on their paracrine activity than their actual incorporation into tissues.[18,19] Extracellular vesicles (EVs) carry genetic material, including microRNAs, and proteins. Thus they are responsible for intercellular communication. They are secreted by most cell types and occur naturally in body fluids including blood, saliva, urine, and breast milk. But cells are known to increase their release following activation.[14] Mesenchymal stem cell-derived vesicles have been shown to have similar properties as functional MSCs. There are reports on their regulatory function on neurite growth,[20] promoting angiogenesis,[21] and reducing myocardial ischemia/reperfusion injury.[22]

The aim of this study was to compare the therapeutic benefit of ADSC derived extracellular vesicles to ADSC on bone repair whereas using ß-TCP biomaterial as a carrier. If similar beneficial effect from EV application alone could be demonstrated this could obviate the risks associated with cell-therapies in regenerative medicine.

MATERIALS AND METHODS

Isolation and Characterization of Adipose Tissue-Derived Stem Cell

Adipose tissue harvested from the inguinal fat pad of 1 rat was washed twice with sterile saline solution supplemented with 1%

Copyright © 2021 Mutaz B. Habal, MD. Unauthorized reproduction of this article is prohibited.

penicilline/streptomycin. The tissue was cut into small pieces in sterile petri dish under laminar flow, adipose tissue was treated with 0.075% type I collagenase for 60 to 120 minutes with vigorous vortexing in every 15 minutes. Homogeneous tissue was then centrifuged twice at 600×g and pellet was maintained in Dulbecco Modified Eagle medium for the stem cell culture. After 24 hours incubation, unattached cells were removed. Cells were routinely cultured with Dulbecco modified Eagle medium containing 10% fetal bovine serum, and 2 mM L-glutamine. The medium was replaced every 3 days and attached cell growth was observed. Cells were passaged when they reached 80% to 90% confluence. Cells were stained with fluorescein isothiocyanate (FITC) and phycoerythrin (PE) labeled antibodies for phenotypic characterization. Antibodies were chosen based on the absence or presence of their reactive antigen on surface. Flow cytometry analyses was performed using a stringent cell gating and multicolor antibody panel including cluster of differentiation (CD)14, CD34, CD45, CD90, and CD105. CD 90 and CD 105 positivity and CD 14, CD34, and CD45 negativity was expected.[16] Nonspesific fluorescence was determined by incubation of similar cells aliquots with iso-type-matched mouse monoclonal antibodies. The cells were washed with PBS and analyzed using the CellQuest program by BD FACS Calibur.

Isolation and Identification of Extracellular Vesicles

After MSC isolation, cells were randomly separated into 2 groups. Cells were kept in FBS free medium during incubation periods to prevent the EVs originated from FBS. One group was incubated in water bath at 42°C for 4 hours. Following incubation, the cultures were left at 37°C for 2 hours. The other group of cells were maintained at 37°C. At the end of incubation, cell media was harvested and centrifuged at 1000 RPM for 15 minutes to remove any cells and debris. EVs were isolated using the Norgen Biotek Cell Culture Media Exosome Isolation Kit according to manufacturer's instructions. Final amount of EVs were 20 μg per animal. All procedures were performed at room temperature. Extracellular vesicles were stored at −80°C until used.

Extracellular vesicles can be characterized by a wide number of techniques and tetraspanins are a group of proteins that can be used for EV characterization. CD9 and CD63 are transmembrane proteins that are commonly found on EV.[21,22] The presence of EV surface marker proteins were analyzed by western blot technique. After isolation, total protein amount of the samples was determined using bicinchroninic acid method. Each well was loaded with 50 μg protein, gels were run at constant V (Volt) for nearly 2 hours. The membrane was blotted with polyvinylidene (PVDF) membrane and blocked with 3% bovine serum albumine (BSA) overnight. Primary and secondary antibodies were incubated with the membrane.

The EV morphology was further confirmed using a scanning electron microscope (EVA MA 10, Zeiss, San Diego, CA) at an accelerating voltage of 10 kV. Samples were coated with gold/palladium (18 nm) using a sputter coater (SC7620, Quorum, Lewes, UK).

Attenuated Total Reflection Fourier-Transform Infrared Spectroscopy

Before implantation, the infrared spectrums of samples were investigated by attenuated total reflection Fourier-transform infrared spectroscopy (FTIR) (FT/IR4700, Jasco, Tokyo, Japan) equipped with a Gladi attenuated total reflection. All spectra were recorded in the region of the wavelength of 400 to 4000 cm^{-1}.

Surgical Procedure

The study was approved by Marmara University Ethics Committee of Experimental Animal Research. Forty male Sprague-Dawley rats weighing between 250 and 300 g were used in this study. Following surgical procedure, the animals were kept in individual cages and received food and water ad libitum. Intraperitoneal injection of 90 mg/kg ketamine (Ketalar) and 10 mg/kg Xylazine (Rompun 2%, bayer) was used for anesthesia.

Two centimeter long skin incision was made on the scalp of each animal. The calvarium was exposed with subperiosteal dissection. A single critical size bone defect of 8 mm in diameter was created on the right side of the calvarium using a custom made punch needle (Trimed, Turkey). Animals were randomly divided into 5 groups:

Group 1: The defect was left untreated
Group 2: The defect was covered with autologous bone graft
Group 3: The defect was filled with ß-TCP granules seeded with ADSC
Group 4: The defect was filled with ß-TCP granules seeded with ADSC-derived EVs
Group 5: The defect was filled with ß-TCP granules

Tricalcium phosphate granules were 140 nm in size. Following surgical intervention the skin was closed with sutures. Eight weeks after surgery, the animals were first put under anesthesia, as described above, for radiologic imaging and later euthanized by decapitation for histologic evaluation.

Radiologic Imaging

Computed tomography imaging was performed on a 256 channel multislice computed tomography scanner (Somatom Flash, Siemens, Erlangen, Germany). Images were acquired sagittally with a slice thickness of 0.6 mm. Afterwards images were reconstructed with the same slice thickness in the axial and coronal planes. Cranial defect density was measured at its widest diameter in all 3 planes and the average density of the newly formed bone was calculated. In group 2 (autologous bone graft) only the area of the newly formed bone between the bone graft and the cranial defect border was calculated. In groups 3, 4, and 5, the density of the granules (range: −190 to −380 Hounsfield Units) were neglected, since their maximum density was below that of fat.

Histologic Evaluation

Previously created surgical site was harvested with surrounding intact bone for histologic evaluation. Bone tissues were fixed in 10% neutral buffered formalin, rinsed with dH_2O and treated with commercial decalcifier (Osteomoll Merck, Massachussetts, USA) for 7 to 10 days. Decalcified bone specimens were dehydrated in ascending alcohol series (70%, 90%, 96%, and 100%), cleared with xylene and then embedded in paraffin. Tissue samples in paraffin blocks were cut approximately 5-μm-thick with a rotary microtome (Leica RM2125RT, Wetzlar, Deutchland) and the sections were stained with hematoxylin and eosin stain for general histologic evaluations and Masson trichome stain (GBL, 5022-100) for examining the bone formation and calcification. Stained sections were evaluated by blinded histologist using a microscope (Olympus BX51, Tokyo, Japan) attached with a camera (Olympus DP72).

Modified histopathologic scoring were evaluated at 40× magnification in 3 similar areas of each section. Vascularization, osteoblastic activity, and trabecular bone formation were scored.[23,24] Cell count for osteoblastic activity were semi-quantitatively scored as; none: 0; 1 to 10 cells: 1; 11 to 20 cells: 2; more than 21 cells: 3 and blood vessel count for vascularization were semi-quantitatively scored as; none: 0; 1 to 5 vessels: 1; 6 to 10 vessels: 2;

© 2021 Mutaz B. Habal, MD
Copyright © 2021 Mutaz B. Habal, MD. Unauthorized reproduction of this article is prohibited.

more than 11 vessels: 3. Trabecular bone formation was scored as none: 0; mild: 1; moderate: 2; dense: 3. Total maximum score was 9.

Statistical Analysis

Histologic data was not normally distributed and the sample sizes were small. Therefore histology data was analyzed using Mann–Whitney *U* test and radiology data were analyzed using Kruskal–Wallis test. Tukey HSD multiple comparisons posthoc test was performed for pair-wise comparisons for each parameter. Differences were considered significant at $P < 0.05$.

RESULTS

Isolation and Characterization of Adipose Derived Stem Cell

Under general culture conditions, adherent cells were observed in several shapes 3 days after seeding. Colonies appeared 7 days after isolation and they reached 80% confluence nearly in 3 weeks. Flow cytometric analysis showed that ADSC were strongly positive for MSC-specific surface-markers including CD 90 (93.9%), CD 105, CD34 after passage 2 (Fig. 1). Cultured cells were negative for CD 14, CD 45 (12.7%, 5.0%, respectively). CD 34 expression was slightly positive (49.0%). Following characterization procedure, 1×10^6ADSC cells were applied per animal in 50 μL.

Characterization of Extracellular Vesicles

The expression of EV surface proteins from both thermo-induced ADSC and non-thermo-induced ADSC was examined using western blot technique. The results of western blot analysis revealed that thermo-induced group expressed surface marker proteins CD9 and CD63 more strongly than the non-thermo-induced group (Fig. 2). Scanning electron microscope imaging showed cup or round shaped morphology with a size ranging from 50 to 150 nm further confirming the presence of EVs (Fig. 3).

Attenuated Total Reflection-Fourier Transform Infrared Spectroscopy

Attenuated total reflection-FTIR spectroscopy was performed to characterize the chemical structures of β-TCP, EV, and β-TCP/EV samples. β-tricalcium phosphate powder showed strong absorption bands at 559 and 1020 cm^{-1} corresponding to stretching vibration of P-O bonding and bending vibration of PO_4^3 group, respectively[25,26] (Fig. 4). The FTIR spectrum of EVs mainly consists of two-branched peaks at 3327 cm^{-1} and 1653 cm^{-1} which belong to overlapped -OH stretching vibration and the N-H stretching

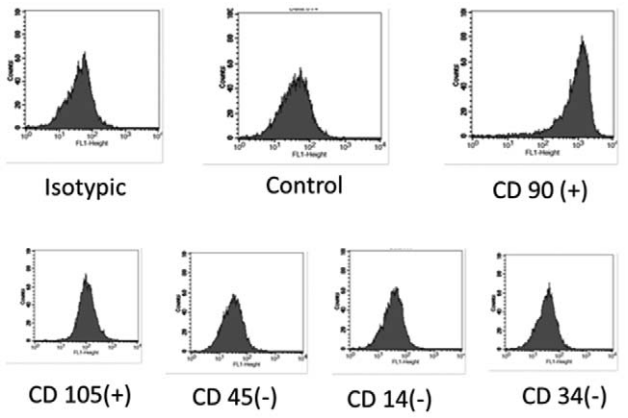


FIGURE 1. Flow cytometry analysis of stem cells.

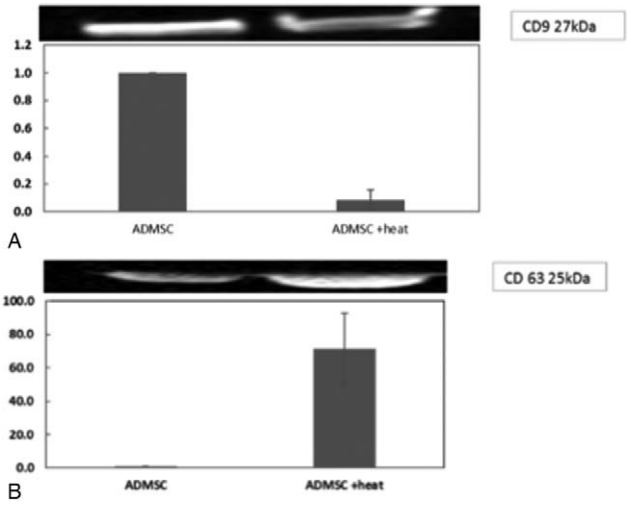


FIGURE 2. Western blot image of extracellular vesicles.

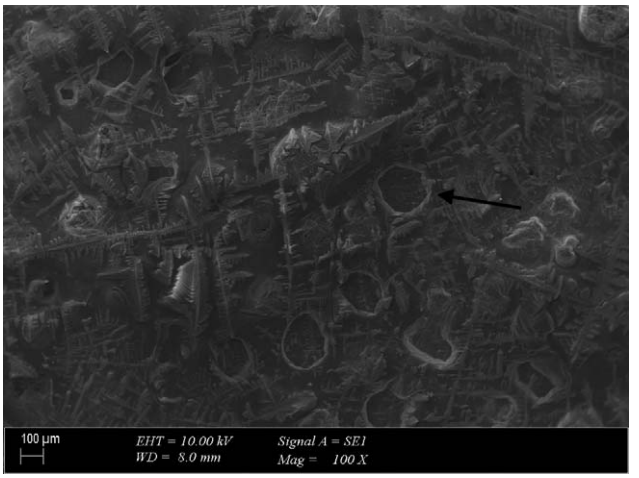


FIGURE 3. Black arrow indicates the scanning electron microscopy image of an extracellular vesicle.

vibrations depending upon Amide A group of proteins and Amide II vibration, respectively.[27] β-TCP/EV sample showed all characteristic peaks both of β-TCP and EV (Fig. 4). These results confirm that EVs were successfully loaded onto β-TCP powder and there

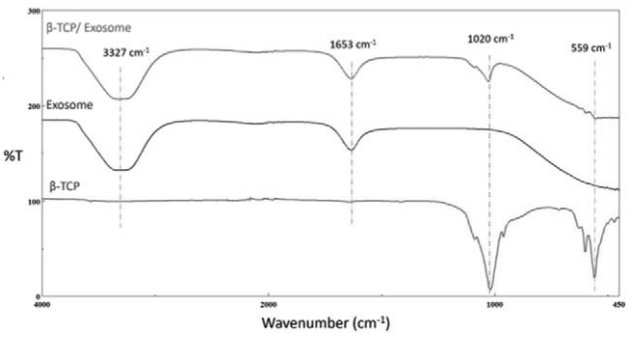


FIGURE 4. FTIR spectroscopy. β-TCP/extracellular vesicle combination showing strong absorption at both β-TCP and extracellular vesicle peaks, indicating successful loading of extracellular vesicle to β-TCP granules. FTIR, Fourier-transform infrared spectroscopy; TCP, tricalcium phosphate

© 2021 Mutaz B. Habal, MD

Copyright © 2021 Mutaz B. Habal, MD. Unauthorized reproduction of this article is prohibited.

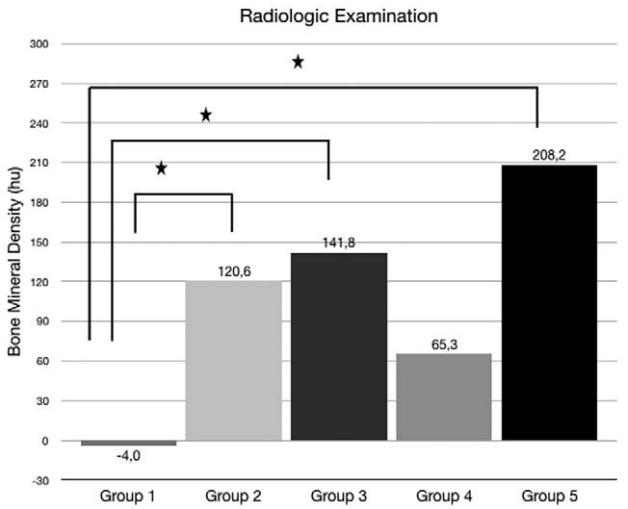


FIGURE 5. Bone mineral density measurements. Stars indicate significant differences.

was no change observed in the chemical structure of the both bioactive component.

Two rats from groups 3, 4, and 5 were not able to complete 8 week follow up period. During histologic examination, we were not able to retrieve wide enough cross-section area for evaluation from 2 rats in groups 1 and 2. Therefore for histologic examination n = 6 for each group.

Radiologic Imaging

The results of bone mineral density are shown in Figure 5. Bone mineral density showed significant differences among groups ($P = 0.0006$). Posthoc test showed that group 2 ($P = 0.01$), group 3 ($P = 0.04$), and group 5 ($P = 0.002$) had significantly higher bone mineral density in compared with group 1 (Fig. 6).

Histologic Evaluation

Abnormally organized tissue matrix with fibrous tissue and some intramembranous ossification areas in early stage of recovery were observed in group 1 (Fig. 7A-B). Wide mineralized area in bone matrix, increase in the number of osteocytes, well-developed canaliculi osseum as indicatives of further stage of recovery were observed in group 2 (Fig. 7C and D). In group 3 (Fig. 7E-F), group 4 (Fig. 7G-H), and group 5 (Fig. 7I-J), the findings were similar as follows, increase in the thickness of trabecular bone with more regular organization, increase in the number of osteocytes located in lacunae when compared with group 1. However group 3 was observed to be at more advanced stages of healing with Haversian canal formation in comparison with group 4 and group 5.

The data of semiquantitative analyses obtained from Masson trichrome stained sections (Fig. 8) showed significantly higher scores for group 2 ($P = 0.02$), group 3 ($P = 0.02$) and group 4 ($P = 0.04$) compared to group 1 (Fig. 9).

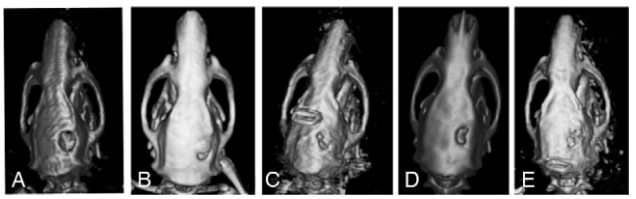


FIGURE 6. 3D images of rat calvarium from garoup 1 (A), group 2 (B), group 3 (C), group 4 (D), group 5 (E). 3D, three-dimensional.

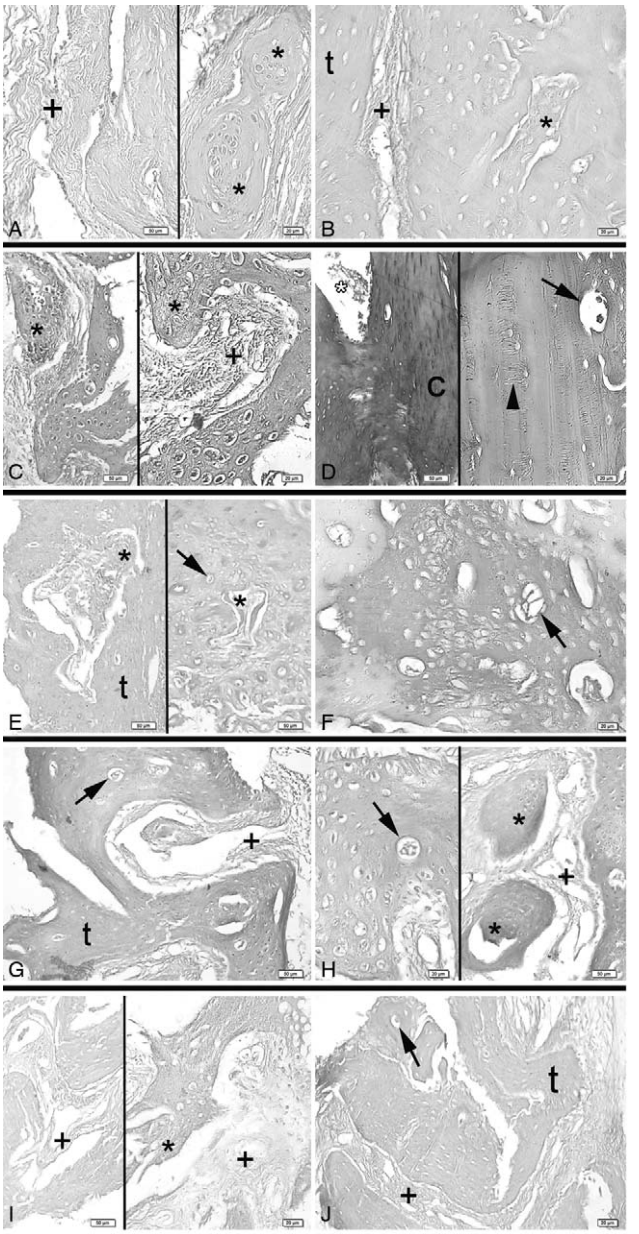


FIGURE 7. Representative photomicrographs of experimental groups. Arrow: Haversian canal. Arrowhead: Canaliculi osseum. Asterisk (*): Intramembraneous ossification. White asterisk: bone marrow. Plus (+): fibrous tissue. t: trabecular bone. c: compact bone. H&E staining.

DISCUSSION

Bone defects following trauma or cancer surgery can be challenging for the reconstructive surgeon. Tissue engineering applications have been studied to overcome potential problems such as donor site availability and morbidity. In the present study, we have compared the effect of ADSC to ADSC-derived EVs combined with ß-TCP on bone healing in a rat calvarial critical size defect model. We have also included a bone graft group which is considered to be the gold standard to repair bone defects.

© 2021 Mutaz B. Habal, MD

Copyright © 2021 Mutaz B. Habal, MD. Unauthorized reproduction of this article is prohibited.

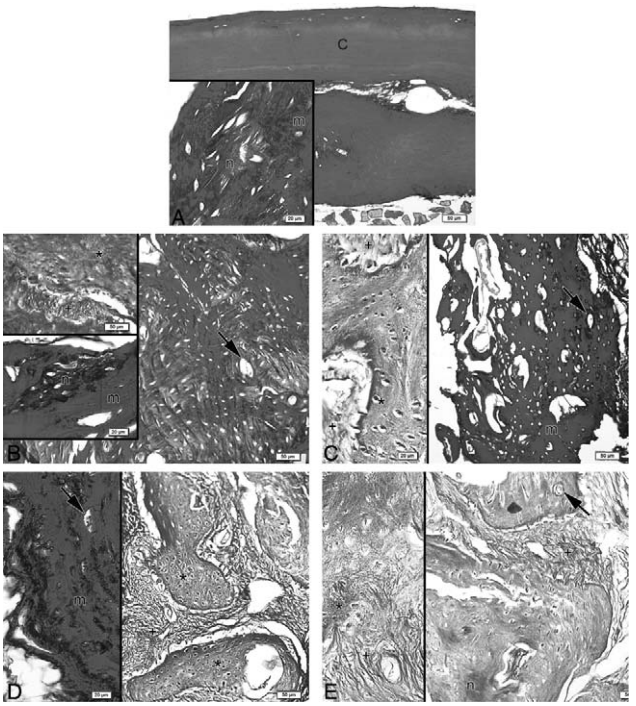


FIGURE 8. Representative photomicrographs of experimental groups. Arrow: Haversian canal. Asterisk (*): intramembraneous ossification. Plus (+): fibrous tissue. c: compact bone. n: nonmineralized bone tissue. m: mineralized bone tissue. Masson trichrome technique stained the calcified bone matrix in red color whereas nonmineralized bone in blue color.

Histologic examination revealed that all treatment groups (groups 2, 3, 4), except group 5, showed significantly better bone regeneration scores than group 1 (no treatment). Although bone regeneration scores between treatment groups were not statistically significant, group 3 (ß-TCP + ADSC) had the highest score and was observed to be at more advanced stages of healing with Haversian canal formation. Gerardo et al[28] have reported that ADSC-loaded ß-TCP without osteogenic differentiation additives still showed alkaline phosphatase, osteopontin, and osteocalcin expression, indicating that ß-TCP alone had the capacity to stimulate ADSC differentiation into osteoblastic phenotype. On the other hand, Feng et al[29] have demonstrated that osteoinduced ADSCs combined with

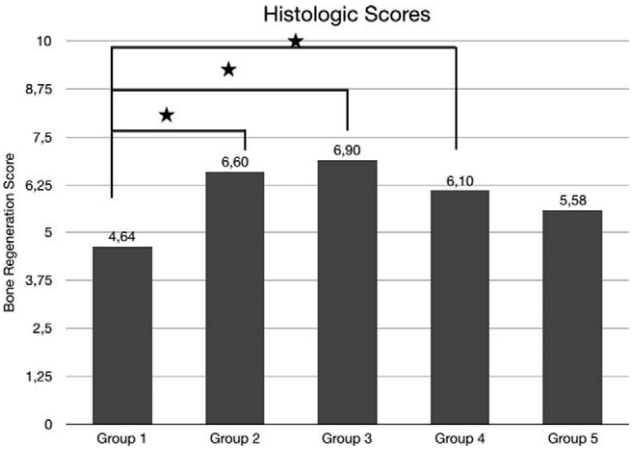


FIGURE 9. Semiquantitative histologic scoring. Stars indicate significant differences.

ß-TCP strongly enhanced the osteoblastic activity in bone defects compared to ß-TCP alone. In the present study, ß-TCP presence may have been inadequate to induce osteoblastic differentiation of ADSCs in a clinical setting and may possibly explain why group 3, although having the highest score and more organized healing pattern, have not shown a statistically significant difference in score compared to group 5. Radiologic examination revealed significantly higher bone mineral density in groups 2, 3, and 5 compared to group 1. However there was not a significant difference between treatment groups.

Extracellular vesicles are considered to play a major role in cell-to-cell communication transferring proteins and carrying functional genetic material.[30–33] Extracellular vesicles are continuously secreted from cells, but their secretion is enhanced following activation. Their release largely depends on the activation of ADSCs by a stress factor. It has been shown by other authors that their amount and content also vary depending on whether they are subjected to stress.[34–36] Based on these information, we have used heat as a stress factor to stimulate EV release.

Exosomes, which are a subset of EVs, isolated from bone marrow derived mesenchymal stem cells (BMSCs) have been combined with ß-TCP for repair of critical size defects.[37]. The authors have shown that their effect largely depended on the total amount of exosomes applied on the biomaterial. Zhang et al[38] have demonstrated that exosomes generated from human induced pluripotent stem cell-derived mesenchymal stem cells (hiPS-MSC) combined with ß-TCP could be released in vitro and later internalized by human BMSCs (hBMSC) and stimulate proliferation, migration and osteogenic differentiation of hBMSCs. Both of these studies used BMSCs as parent cells and source of exosomes. In the present study we have used ADSCs, which are more easily retrievable and found in abundance throughout the body. Also, the previously mentioned studies compare the therapeutic effect of different amounts of exosomes rather than comparing their effect to their parent cell. Here we demonstrated, although bone repair in ADSC and EV applied groups (group 3 versus group 4) were not histologically or radiologically different, group 3 showed more advanced healing. This may be explained in several ways. Extracellular vesicle effect may depend on the total amount applied as mentioned in other studies.[37] The fact that ADSC applied group was in more advanced stages of healing may imply that stem cells have other ways of communicating to induce regeneration. Another explanation to how application of ß-TCP/ADSC and ß-TCP/EV generated similar osteogenic activity as application of ß-TCP alone is that ß-TCP may have failed to stimulate osteogenic differentiation of ADSCs. Hence, it could potentially be more beneficial to treat ADSCs in an osteogenic medium before their application.

The presence of EVs on ß-TCP was only confirmed, in vitro, using spectroscopy. Similar to other studies in the field,[37,38] we have not checked if the EVs remain in place after implantation of ß-TCP/EV combination into the defects. However, Zhang et al have confirmed, in vitro, that labeled exosomes placed in culture plates containing hBMSC were taken up by these cells and were present in their perinuclear regions. This seems to be the main mechanism of action of exosomes. It is also known that endogenous BMSCs can be mobilized in response to injury and act as the main cells in bone repair.[39] Therefore any osteogenic activity generated by the EVs in this study most likely depended on their uptake by endogenous stem cells.

CONCLUSIONS

Direct application of stem cells remains controversial. The demonstration of the importance of extracellular vesicles in cell-to cell communication and the fact that MSCs act mostly via paracrine

© 2021 Mutaz B. Habal, MD

Copyright © 2021 Mutaz B. Habal, MD. Unauthorized reproduction of this article is prohibited.

activity are all promising for future use of these vesicles in certain therapies. However further studies are needed to determine the optimal amount and content of EVs required to activate the target cells.

REFERENCES

1. Trisi P, Rao W, Rebaudi A, et al. Histologic effect of pure-phase beta-tricalcium phosphate on bone regeneration in human artificial jawbone defects. *Int J Periodontics Restorative Dent* 2003;23:69–77
2. Zhou H, Xiao C, Wang Y, et al. In vivo efficacy of bone marrow stromal cells coated with beta-tricalcium phosphate for the reconstruction of orbital defects in canines. *Invest Ophthalmol Vis Sci* 2011;52:1735–1741
3. Katagiri W, Osugi M, Kawai T, et al. First-in-human study and clinical case reports of the alveolar bone regeneration with the secretome from human mesenchymal stem cells. *Head Face Med* 2016;12:5
4. Han P, Xu M, Chang J, et al. Lithium release from β-tricalcium phosphate inducing cementogenic and osteogenic differentiation of both hPDLCs and hBMSCs. *Biomater Sci* 2014;2:1230–1243
5. Yuan H, Fernandes H, Habibovic P, et al. Osteoinductive ceramics as a synthetic alternative to autologous bone grafting. *Proc Natl Acad Sci U S A* 2010;107:13614–13619
6. Gupta A, Leong DT, Bai HF, et al. Osteo-maturation of adipose-derived stem cells required the combined action of vitamin D3, (-glycerophosphate, and ascorbic acid. *Biochem Biophys Res Commun* 2007;362:17–24
7. Gersbach CA, Byers BA, Pavlath GK. Runx2/Cbfa1 stimulates transdifferentiation of primary skeletal myoblasts into a mineralizing osteoblastic phenotype. *Exp Cell Res* 2004;300:406–417
8. Dravida S, Pal R, Khanna A, et al. The transdifferentiation potential of limbal fibroblast-like cells. *Brain Res Dev Brain Res* 2005;160:239–251
9. Kosmacheva SM, Volk MV, Yeustratenka TA, et al. In vitro growth of human umbilical blood mesenchymal stem cells and their differentiation into chondrocytes and osteoblasts. *Bull Exp Biol Med* 2008;145:141–145
10. Buranasinsup S, Sila-Asna M, Bunyaratvej N, et al. In vitro osteogenesis from human skin-derived precursor cells. *Dev Growth Differ* 2006;48:263–269
11. Yagami K, Uyama Y, Yoshizawa Y, et al. A human chondrogenic cell line retains multi-potency that differentiates into osteoblasts and adipocytes. *Bone* 2004;34:648–655
12. Lansley SM, Searles RG, Hoi A, et al. Mesothelial cell differentiation into osteoblast and adipocyte-like cells. *J Cell Mol Med* 2011;15:2095–2105
13. Oki Y, Ono H, Motohashi T, et al. Dedifferentiated follicular granulosa cells derived from pig ovary can transdifferentiate into osteoblasts. *Biochem J* 2012;447:239–248
14. Baglio SR, Pegtel DM, Baldini N. Mesenchymal stem cell secreted vesicles provide novel opportunities in (stem) cell-free therapy. *Front Physiol* 2012;3:359:1–11
15. Liang X, Ding Y, Zhang Y, et al. Paracrine mechanisms of mesenchymal stem cell-based therapy: current status and perspectives. *Cell Transplant* 2014;23:1045–1059
16. Pittenger MF, Mackay AM, Beck SC, et al. Multilineage potential of adult human mesenchymal stem cells. *Science* 1999;284:143–147
17. Marino G, Rosso F, Cafiero G, et al. β-Tricalcium phosphate 3D scaffold promote alone osteogenic differentiation of human adipose stem cells. *J Mater Sci Mater Med* 2010;21:353–363
18. Rosario CM, Yandava BD, Kosaras B, et al. Differentiation of engrafted multipotent neural progenitors towards replacement of missing granule neurons in meander tail cerebellum may help determine the locus of mutant gene action. *Development* 1997;124:4213–4224
19. Li TS, Takahashi M, Ohshima M, et al. Myocardial repair achieved by the intramyocardial implantation of adult cardiomyocytes in combination with bone marrow cells. *Cell Transplant* 2008;17:695–703
20. Xin H, Li Y, Buller B, et al. Exosome-mediated transfer of miR-133b from multipotent mesenchymal stromal cells to neural cells contributes to neurite outgrowth. *Stem Cells* 2012;30:1556–1564
21. Zhang HC, Liu XB, Huang S, et al. Microvesicles derived from human umbilical cord mesenchymal stem cells stimulated by hypoxia promote angiogenesis both in vitro and in vivo. *Stem Cells Dev* 2012;21:3289–3297
22. Lai RC, Arslan F, Lee MM, et al. Exosome secreted by MSC reduces myocardial ischemia/reperfusion injury. *Stem Cell Res* 2010;4:214–222
23. Toker H, Ozdemir H, Ozer H, et al. Alendronate enhances osseous healing in a rat calvarial defect model. *Arch Oral Biol* 2012;57:1545–1550
24. Sun D, Chen Y, Tran RT, et al. Citric acid-based hydroxyapatite composite scaffolds enhance calvarial regeneration. *Sci Rep* 2014;4:6912:1–9
25. Yusof MR, Shamsudin R, Zakaria S, et al. Fabrication and characterization of carboxymethyl starch/poly(l-lactide) acid/β-tricalcium phosphate composite nanofibers via electrospinning. *Polymers (Basel)* 2019;11:1468:1–16
26. Liga Berzina-Cimdina, Natalija Borodajenko. Research of Calcium Phosphates Using Fourier Transform Infrared Spectroscopy, Infrared Spectroscopy - Materials Science, Engineering and Technology, Prof. Theophanides Theophile (Ed.), 2012. ISBN: 978-953-51-0537-4, InTech, Available from: http://www.intechopen.com/books/infrared-spectroscopy-materials-science-engineering-and-technology/research-of-calcium-phosphates-using-fourier-transformation-infrared-spectroscopy
27. Mihály J, Deák R, Szigyártó IC, et al. Characterization of extracellular vesicles by IR spectroscopy: fast and simple classification based on amide and CH stretching vibrations. *Biochim Biophys Acta Biomembr* 2017;1859:459–466
28. Marino G, Rosso F, Cafiero G, et al. β-Tricalcium phosphate 3D scaffold promote alone osteogenic differentiation of human adipose stem cells: in vitro study. *J Mater Sci: Mater Med* 2010;21:353–363
29. Feng W, Lv S, Cui J, et al. Histochemical examination of adipose derived stem cells combined with β-TCP for bone defects restoration under systemic administration of 1α,25(OH) 2 D 3. *Materials Science and Engineering: C* 2015;54:133–141
30. Ratajczak J, Miekus K, Kucia M, et al. Embryonic stem cell-derived microvesicles reprogram hematopoietic progenitors: evidence for horizontal transfer of mRNA and protein delivery. *Leukemia* 2006;20:847–856
31. Valadi H, Ekström K, Bossios A, et al. Exosome-mediated transfer of mRNAs and microRNAs is a novel mechanism of genetic exchange between cells. *Nat Cell Biol* 2007;9:654–659
32. Skog J, Würdinger T, van Rijn S, et al. Glioblastoma microvesicles transport RNA and proteins that promote tumour growth and provide diagnostic biomarkers. *Nat Cell Biol* 2008;10:1470–1476
33. Pegtel DM, Cosmopoulos K, Thorley-Lawson DA, et al. Functional delivery of viral miRNAs via exosomes. *Proc Natl Acad Sci U S A* 2010;107:6328–6333
34. Parolini I, Federici C, Raggi C, et al. Microenvironmental pH is a key factor for exosome traffic in tumor cells. *J Biol Chem* 2009;284:34211–34222
35. Hedlund M, Nagaeva O, Kargl D, et al. Thermal- and oxidative stress causes enhanced release of NKG2D ligand-bearing immunosuppressive exosomes in leukemia/lymphoma T and B cells. *PLoS One* 2011;6:e16899:1–10
36. Lv LH, Wan YL, Lin Y, et al. Anticancer drugs cause release of exosomes with heat shock proteins from human hepatocellular carcinoma cells that elicit effective natural killer cell antitumor responses in vitro. *J Biol Chem* 2012;287:15874–15885
37. Qi X, Zhang J, Yuan H, et al. Exosomes secreted by human-induced pluripotent stem cell-derived mesenchymal stem cells repair critical-sized bone defects through enhanced angiogenesis and osteogenesis in osteoporotic rats. *Int J Biol Sci* 2016;12:836–849
38. Zhang J, Liu X, Li H, et al. Exosomes/tricalcium phosphate combination scaffolds can enhance bone regeneration by activating the PI3K/Akt signaling pathway. *Stem Cell Res Ther* 2016;7:136:1–14
39. Deschaseaux F, Sensebe L, Heymann D. Mechanisms of bone repair and regeneration. *Trends Mol Med* 2009;15:417–429

© 2021 Mutaz B. Habal, MD

Copyright © 2021 Mutaz B. Habal, MD. Unauthorized reproduction of this article is prohibited.